



Article

Numerical Analysis of Natural Convection Driven Flow of a Non-Newtonian Power-Law Fluid in a Trapezoidal Enclosure with a U-Shaped Constructal

Sardar Bilal¹, Maryam Rehman¹, Samad Noeiaghdam^{2,3} , Hijaz Ahmad^{4,5,*}  and Ali Akgül⁶

¹ Department of Mathematics, Air University, P.A.F Complex E-9, Islamabad 44000, Pakistan; sardarbilal@mail.au.edu.pk (S.B.); maryamrehman788@gmail.com (M.R.)

² Industrial Mathematics Laboratory, Baikal School of BRICS, Irkutsk National Research Technical University, 664074 Irkutsk, Russia; noiagdams@susu.ru

³ Department of Applied Mathematics and Programming, South Ural State University, Lenin Prospect 76, 454080 Chelyabinsk, Russia

⁴ Section of Mathematics, International Telematic University Uninettuno, Corso Vittorio Emanuele II 39, 00186 Roma, Italy

⁵ Mathematics in Applied Sciences and Engineering Research Group, Scientific Research Center, Al-Ayen University, Nasiriyah 64001, Iraq

⁶ Department of Mathematics, Art and Science Faculty, Siirt University, Siirt 56100, Turkey; aliakgul@siirt.edu.tr

* Correspondence: hijaz555@gmail.com



Citation: Bilal, S.; Rehman, M.; Noeiaghdam, S.; Ahmad, H.; Akgül, A. Numerical Analysis of Natural Convection Driven Flow of a Non-Newtonian Power-Law Fluid in a Trapezoidal Enclosure with a U-Shaped Constructal. *Energies* **2021**, *14*, 5355. <https://doi.org/10.3390/en14175355>

Academic Editor: Jose A. Almendros-Ibanez

Received: 20 June 2021

Accepted: 22 August 2021

Published: 28 August 2021

Publisher's Note: MDPI stays neutral with regard to jurisdictional claims in published maps and institutional affiliations.



Copyright: © 2021 by the authors. Licensee MDPI, Basel, Switzerland. This article is an open access article distributed under the terms and conditions of the Creative Commons Attribution (CC BY) license (<https://creativecommons.org/licenses/by/4.0/>).

Abstract: Placement of fins in enclosures has promising utilization in advanced technological processes due to their role as heat reducing/generating elements such as in conventional furnaces, economizers, gas turbines, heat exchangers, superconductive heaters and so forth. The advancement in technologies in power engineering and microelectronics requires the development of effective cooling systems. This evolution involves the utilization of fins of significantly variable geometries enclosed in cavities to increase the heat elimination from heat-generating mechanisms. Since fins are considered to play an effective role in the escalation of heat transmission, the current study is conducted to examine the transfer of heat in cavities embedding fins, as well as the effect of a range of several parameters upon the transmission of energy. The following research is supplemented with the interpretation of the thermo-physical aspects of a power-law liquid enclosed in a trapezoidal cavity embedding a U-shaped fin. The Boussinesq approximation is utilized to generate the mathematical attributes of factors describing natural convection, which are then used in the momentum equation. Furthermore, the Fourier law is applied to formulate the streaming heat inside the fluid flow region. The formulated system describing the problem is non-dimensionalized using similarity transformations. The geometry of the problem comprises a trapezoidal cavity with a non-uniformly heated U-shaped fin introduced at the center of the base of the enclosure. The boundaries of the cavity are at no-slip conditions. Non-uniform heating is provided at the walls (l_1 and l_2), curves (c_1 , c_2 and c_3) and surfaces (s_1 and s_2) of the fin; the upper wall is insulated whereas the base and sidewalls of the enclosure are kept cold. The solution of the non-dimensionalized equations is procured by the Galerkin finite element procedure. To acquire information regarding the change in displacement w.r.t time and temperature, supplementary quadratic interpolating functions are also observed. An amalgam meshing is constructed to elaborate the triangular and quadrilateral elements of the trapezoidal domain. Observation of significant variation in the flow configurations for a specified range of parameters is taken into consideration i.e., $0.5 \leq n \leq 1.5$ and $10^4 \leq Ra \leq 10^6$. Furthermore, flow structures in the form of velocity profiles, streamlines, and temperature contours are interpreted for the parameters taken into account. It is deduced from the study that ascending magnitude of (Ra) elevates level of kinetic energy and magnitude of heat flux; however, a contrary configuration is encapsulated for the power-law index. Navier–Stokes equations constituting the phenomenon are written with the help of non-dimensionalized stream function, temperature profiles, and vortices, and the solutions are acquired using the finite element method. Furthermore, the attained outcomes are accessible through velocity and temperature profiles. It is worth highlighting the fact that the following analysis enumerates the pseudo-plastic, viscous and dilatant behavior of

the fluid for different values of (n). This study highlights that the momentum profile and the heat transportation increase by increasing (Ra) and decline as the viscosity of the fluid increases. Overall, it can be seen from the current study that heat transportation increases with the insertion of a fin in the cavity. The current communication signifies the phenomenon of a power-law fluid flow filling a trapezoidal cavity enclosing a U-shaped fin. Previously, researchers have studied such phenomena mostly in Newtonian fluids, hence the present effort presents novelty regarding consideration of a power-law liquid in a trapezoidal enclosure by the placement of a U-shaped fin.

Keywords: power-law fluid; trapezoidal cavity; U-shaped fin; free convection; non-uniform heating; finite element method

1. Introduction

The study of physical geometries for the formation of constructal designs for industrial and engineering sectors has been globally attractive and has invited experts involved in its development. This progress was initiated by placing multiple shaped cylinders for augmentation and controlling of the heat, specifically in thermally controlled systems. Placement of fins in enclosures has promising utilization in advanced technological processes such as conventional furnaces, economizers, gas turbines, heat exchanges, and superconductive heaters as heat reducing/generating elements, effectively obligatory in recent years.

The placement of thermally conducted fins such as heated cylinders in thermodynamic systems brings about evolution in the construction of vast industrial designs [1,2]. Fins add a promising role in engineering and applied science configurations such as conventional furnaces, economizers, gas turbines, heat exchanges, superconductive heaters, and so forth. Fins also control the economic cost of transmission of heat along with improving quality in different heating sources. Readers are referred to [3–8] for a critical overview of the advantages of fins and their effective role. In recent years, an extensive literature has appeared regarding heat generation and control by utilizing fins in different shaped enclosures. For the sake of interest, some of these are successively mentioned. Shi and Khodadadi [9] analyzed the capability of heat transportation inside a heated squared enclosure by anchoring a thin fin. They concluded that a significant amount of heat is deposited in the presence of the fin in contrast to a situation when the fin is not located inside the cavity. Horbach et al. [10] applied a Y-shaped constructal design to facilitate heat passage in a highly heat-conductive material inserted in a squared cavity. Rehman et al. [11] made a noticeable attempt to investigate the buoyantly convective flow of a non-Newtonian liquid in a rhombus-shaped cavity with a T-shaped piece of equipment inserted in the domain. Tavana et al. [12] demonstrated heat transportation in the presence of three different fins (rectangular, T, triangular) in a microchannel configuration. They indicated that a triangular fin is very efficient in transporting energy in a channel. Free convection inside a non-uniformly heated domain, with the placement of fins conducting heat on the cold walls of the cavity, was reported by Frederick and Scozia [13]. Flow patterns against high Nusselt number magnitudes at the location of thermally heated fins, also dependent on the magnitude of the Rayleigh number, were adumbrated by Facas et al. [14]. Nag et al. [15] noticed a change in recirculating flow patterns against variation in an aspect ratio of encapsulated fins along with readings of fluctuation of the Rayleigh number in a rectangular cavity.

Filling enclosures with materials possessing pervasive characteristics is highly essential. Before the arrival of the non-Newtonian fluid rheology concept, most of the cavities were filled with air, water, or Newtonian fluids. Eventually, advancement in material testing led the researchers towards fluids that disobeyed Newton's law of viscosity, known as non-Newtonian liquids. Non-Newtonian fluids are mostly recommended in industrial and mechanical procedures due to their huge practical utility. The analysis of non-Newtonian fluids gains special attention due to the non-linear relation of stress and strain which makes

them more appealing to industry. Since dynamic viscosity changes with the application of stress, complication related to non-Newtonian fluid arises, and the flexibility of such fluids varies differently against stress. Hence, these liquids are classified into diversified categories, namely shear-thinning, shear-thickening, and Newtonian fluids. Based on these classifications, researchers have proposed several groups of liquids expressing the class of materials mentioned. Among these, the power-law fluid model is the most generalized, which expresses characteristics of almost all the classified versions by setting various magnitudes of (n) . Besides, examination of non-Newtonian fluids in enclosures is crucial in the processing of food, drilling of oil, geophysical structures' polymeric engineering, electronic preservation systems, nuclear reactors, etc. Perhaps Ozoe and Churchill [16] were the first who depicted hydrodynamical features of a power-law liquid in a shallow horizontal enclosure by evaluating recirculation generated in the fluid flow domain. Kaddiri et al. [17] described the study of a computational scheme for analyzing momentum features of a power-law fluid, inside a square enclosure, along with the finding of the critical magnitude of (n) which differentiate its shear-thinning and thickening attributes. Kim et al. [18] deliberated on the transient flow of power-law fluid in a vertical-cavity along with simultaneity of heat transfer generated through natural convection.

Lamsaadi et al. [19] worked on examining flow attributes of power-law fluid by varying aspect ratios of a shallow domain and also checked the case sensitivity of the power-law index by finding the impact of flow field circulations. Lamsaadi et al. [20] explicated the movement of a power-law liquid in a rotated slit and measured the dramatic effect on cavity rotation, along with model controlling parameters, on the motion of the fluid.

Gravity differences are a driving agent for producing flows in containers. This is due to the production of heavier and lighter particles in the flow domain, due to lower or higher effectivity of gravity forces. The process of such flow circulation is called convection. These gravitational forces create dense and light layers among fluid streams and temperature gradient is automatically generated through natural collision, termed natural convection. The phenomenon of naturally convected flows has typical applications in processing types of equipment such as computer chips, solar paneling, wind chiller, hydraulic pumps, molten metals, heat dissipation fins, and hydrothermal reservoirs. Turan et al. [21] used a commercial package to simulate the buoyant flows driven inside power-law liquid within a cavity, with provision of constant temperature at the walls. Rudolf [22] elucidated the thermodynamical attributes executed in a power-law fluid by generating free convection in an enclosure whose sidewalls are isothermal and whose base is adiabatic. They measured no change in heat transfer against the power-law model variable (n) . The process of convective currents produced due to temperature gradients in rectangular [23] and square [24] enclosures has been accessed. They demarcated the influential significance of (n) and (Ra) on heat transfer and flow field properties, and noticed a critical magnitude of (n) for which heat flux does not vary against the Prandtl number. Alloui [25] discussed free convection in non-Newtonian liquid within an upright enclosure filled with Carreau-Yasuda fluid and constructed a comparison of attained outcomes with a Newtonian case by restricting associated model parameters. They found a very minute change in heat transfer against flow-related variables for the lower magnitude of the Rayleigh number. Ouertatani et al. [26] numerically assessed Rayleigh-Benard convection within a rectangular domain and yielded uniformness in streamlines and isothermal patterns for the magnitude of the Rayleigh number approaching 100. Some recent development in this direction are addressed and accessed in [27–38]. Usman et al. [39] studied the transportation of heat within a power-law liquid in the presence of a sinusoidal heat sink/source between stretchable disks separated with a constant gap and rotating co-axially. They have also performed an analysis of 3D steady flow and heat transportation of a non-Newtonian nano-liquid above stretchable gyrating disks [40]. Usman et al. have also contributed towards the analysis of 3D heat transportation and liquid flow in a Carreau liquid in between rotatory stretchable disks [41]. Furthermore, they have explored the rheological consequences of

a nanofluid over the surface of a Riga plate implanted in a porous medium [42]. Most recently, Usman et al. have communicated transportation of heat in a hyperbolic fluid over a lubricated stretchable rotatory surface of a disk [43]. Goodarzi et al. [44] measured the convective heat transportation in a shallower chamber by incorporating two phasic nano models. Goodarzi et al. [33–38] jointly executed comparative analysis regarding accurate findings for heat flux calculation by utilizing different numerical techniques. A numerical analysis of MHD natural convective fluid flow enclosed between two h-distance apart plates was studied by Rasool et al. [39] Safaei et al. [40] numerically deliberated free convective heat transfer fluid flow inside an elliptical container with varied attack angles. A numerical examination of free convective MHD fluid flow governed by a non-linear stretchable sheet was addressed by Rasool et al. [41]. Recent literature regarding heat transfer aspects in different physical domains is gathered in [42–52].

The prime motivation behind the current research is to analyze attributes of non-Newtonian fluid, flowing in a square enclosure with placement of fins generated by temperature differences. So far, much of the literature regards natural convection in cavities, but for placement of fins very sparse work has been presented. Our purpose is to fill this gap and attract researchers in this direction instead of placing obstacles in enclosures. For this purpose, power-law fluid is utilized and a T-shaped fin is placed at the base of the enclosure. The mathematical articulation of the considered problem is dealt with in the form of partial differential expressions and solved computationally by implementing the finite element method. Initially, discretization of the domain is manifested by distributing it into triangular and rectangular elements. Graphical representations for velocity, temperature, heat flux, and kinetic energy are elaborated along with statistical data about the elements and the relevant physical quantities. A comparison of current work with the published literature is also presented. It is hoped that this research work will assist researchers working in this field.

In the current research, natural convective heat transportation analysis is conducted in a trapezium shaped cavity enclosing a U-shaped fin. Uniform heating is supplied to the fin structure, due to which singularity is observed in the solutions. The significance of the investigation is to observe the heat transportation that seems to increase due to insertion of the fin in the domain. Power-law fluid is also submerged in the cavity to study the effects of variation in viscosity upon fluid flow. To acquire solutions to the problem, the Galerkin finite element method is used. The domain is discretized into triangles and quadrilaterals, i.e., hybrid meshing is attained. According to the results, the power-law catalogue ranging from $0.5 \leq n \leq 1.5$ shows a decrease in momentum profile and kinetic energy as it increases, hence increasing the viscosity of the fluid. Besides, the Rayleigh number $10^4 \leq Ra \leq 10^6$ depicts the increase in the momentum profile, heat transportation and kinetic energy as it ascends. The conclusive remarks that can be drawn from the study are that the heat transportation in a cavity enclosing a fin is greater compared to a cavity without a fin [37].

Despite the great number of applications of placement of multi-shaped fins in enclosures, such a study has not been conducted so far. From the detailed view of the literature earlier, it is seen that heat transportation in a trapezoidal enclosure, cavities enclosing fins and heat transfer in a power-law liquid have been studied separately. The study of thermodynamical aspects of a non-Newtonian liquid in a trapezoidal cavity enclosing a U-shaped fin has not yet been conducted. Influenced by this literature, the current paper describes the thermos-physical attributes of a shear dependent fluid enclosed in a trapezium shaped enclosure embedding a U-shaped fin. Hence, to fill the gap the following analysis is accomplished. This document is organized in the following way: firstly, we present the mathematical modeling and numerical computation of the problem, then the methodology is described, results and discussion are detailed and conclusive remarks are summarized.

2. Mathematical Modelling

The current research is conducted assuming a two-dimensional, time-independent, and steady flow for a shear dependent fluid enclosed in a trapezoidal enclosure. A non-uniformly heated fin shaped like a tuning fork (U-shaped) is inserted in the cavity at the base in order to portray an application of the considered problem, i.e., centrally heated systems and insertions of fin-shaped hindrances. The boundaries of the domain, as well as the flipper, are at the no-slip condition. The fin acts as a non-uniform heat generator whereas the other walls are reserved at low temperature and the upper partition is adiabatic. The Boussinesq approximation buoyancy expression is included in the mathematical formulation of the problem, while all the other physical measures are considered to be at rest. The Boussinesq approximations incorporate the role of free convection in the fluid flow domain. A schematic illustration of the problem is demonstrated in Figure 1.

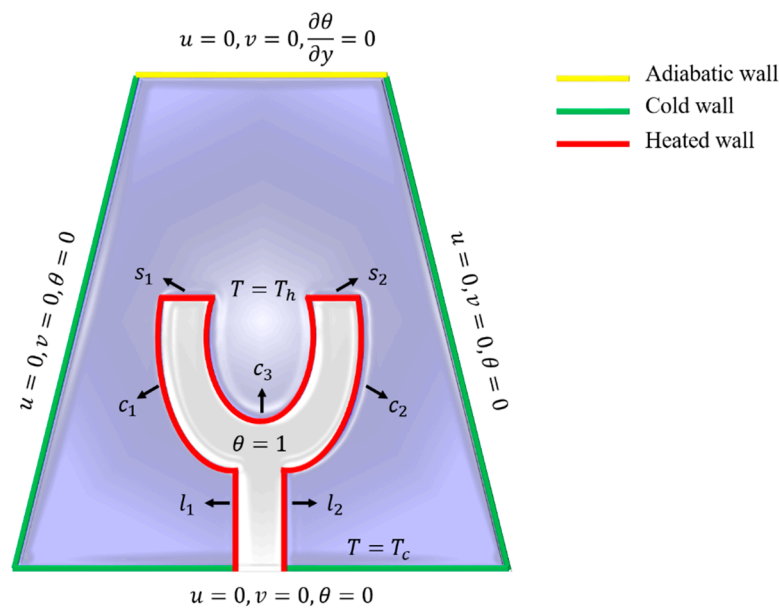


Figure 1. A diagrammatic illustration of the problem.

The equations governing the problem are the continuity equation, momentum equations, and energy expression [53] as follows:

$$\frac{\partial u}{\partial x} + \frac{\partial v}{\partial y} = 0, \quad (1)$$

$$\rho(u \frac{\partial u}{\partial x} + v \frac{\partial u}{\partial y}) = -\frac{\partial p}{\partial x} + \frac{\partial \tau_{xx}}{\partial x} + \frac{\partial \tau_{xy}}{\partial y}, \quad (2)$$

$$\rho(u \frac{\partial v}{\partial x} + v \frac{\partial v}{\partial y}) = -\frac{\partial p}{\partial y} + \frac{\partial \tau_{xy}}{\partial x} + \frac{\partial \tau_{yy}}{\partial y} + \rho g \beta (T - T_c), \quad (3)$$

$$u \frac{\partial T}{\partial x} + v \frac{\partial T}{\partial y} = \alpha \left(\frac{\partial^2 T}{\partial x^2} + \frac{\partial^2 T}{\partial y^2} \right) \quad (4)$$

The stress tensor of viscosity for the power-law fluid is communicated below,

$$\tau_{ij} = 2\mu_a D_{ij} = \mu_a \left(\frac{\partial u_i}{\partial x_j} + \frac{\partial u_j}{\partial x_i} \right) \quad (5)$$

Here, D_{ij} is the strain rate tensor for Cartesian coordinates (two-dimensional) and μ_a is the apparent viscosity derived from the succeeding relation,

$$\mu_a = K \left\{ 2 \left[\left(\frac{\partial u}{\partial x} \right)^2 + \left(\frac{\partial v}{\partial y} \right)^2 \right] + \left(\frac{\partial v}{\partial x} + \frac{\partial u}{\partial y} \right)^2 \right\}^{\frac{n-1}{2}}, \quad (6)$$

The variable K denotes the consistency index and n denotes the power-law constant comprising three cases; ($n < 1$) shear thinning, Newtonian behavior for ($n = 1$) and ($n > 1$) for shear thickening. The supplementary boundary constraints are as follows,

$$\begin{aligned} u(x, 0) = v(x, 0) = 0, \quad 0 \leq x \leq L, \quad y = 0, \\ u(x, y) = v(x, y) = 0, \quad 0 \leq x \leq 0.25, \quad 0 \leq y \leq L, \quad y = \frac{L}{0.25}x, \\ u(x, L) = v(x, L) = 0, \quad 0.25 \leq x \leq 0.75, \quad y = L, \\ u(x, y) = v(x, y) = 0, \quad 0.75 \leq x \leq L, \quad 0 \leq y \leq L, \quad y = \frac{L(L-x)}{L} - 0.75, \end{aligned} \quad (7)$$

Following are the applied similarity variables for the non-dimensionalization of governing expressions in Equations (10)–(13),

$$X = \frac{x}{L}, \quad Y = \frac{y}{L}, \quad U = \frac{uL}{\alpha}, \quad V = \frac{vL}{\alpha}, \quad (8)$$

$$P = \frac{pL^2}{\rho\alpha^2}, \quad \theta = \frac{T - T_c}{\Delta T}, \quad \Delta T = \frac{qL}{k}, \quad (9)$$

The attained dimensionless expressions are as follows,

$$\frac{\partial U}{\partial X} + \frac{\partial V}{\partial Y} = 0 \quad (10)$$

$$U \frac{\partial U}{\partial X} + V \frac{\partial U}{\partial Y} = -\frac{\partial P}{\partial X} + \text{Pr} \left[2 \frac{\partial}{\partial X} \left(\mu_a^* \frac{\partial U}{\partial X} \right) + \frac{\partial}{\partial Y} \left(\mu_a^* \left(\frac{\partial U}{\partial Y} + \frac{\partial V}{\partial X} \right) \right) \right], \quad (11)$$

$$U \frac{\partial V}{\partial X} + V \frac{\partial V}{\partial Y} = -\frac{\partial P}{\partial Y} + \text{Pr} \left[2 \frac{\partial}{\partial Y} \left(\mu_a^* \frac{\partial V}{\partial Y} \right) + \frac{\partial}{\partial X} \left(\mu_a^* \left(\frac{\partial U}{\partial Y} + \frac{\partial V}{\partial X} \right) \right) \right] + Ra \text{Pr} \theta, \quad (12)$$

$$U \frac{\partial \theta}{\partial X} + V \frac{\partial \theta}{\partial Y} = \frac{\partial^2 \theta}{\partial X^2} + \frac{\partial^2 \theta}{\partial Y^2}, \quad (13)$$

Following is μ_a^* , defined to be the apparent non-dimensionalized viscosity,

$$\mu_a^* = \left[2 \left\{ \left(\frac{\partial U}{\partial X} \right)^2 + \left(\frac{\partial V}{\partial Y} \right)^2 \right\} + \left(\frac{\partial V}{\partial X} + \frac{\partial U}{\partial Y} \right)^2 \right]^{\frac{n-1}{2}} \quad (14)$$

The non-dimensionalized form of boundary conditions are:

$$\begin{aligned} U(X, 0) = V(X, 0) = 0, \quad 0 \leq X \leq 1, \quad Y = 0, \\ U(X, Y) = V(X, Y) = 0, \quad 0 \leq X \leq 0.25, \quad 0 \leq Y \leq 1, \quad Y = \frac{X}{0.25} \\ U(X, 1) = V(X, 1) = 0, \quad 0.25 \leq X \leq 0.75, \quad Y = 1, \\ U(X, Y) = V(X, Y) = 0, \quad 0.75 \leq X \leq 1, \quad 0 \leq Y \leq 1, \quad Y = \frac{1-X}{0.25}, \end{aligned} \quad (15)$$

The non-dimensionalization of the coupled governing equations gives rise to the introduction of the following dimensionless parameters,

$$Ra = \frac{\rho g \beta \Delta T L^{2n+1}}{\alpha^n K}, \quad Pr = \frac{KL^{2-2n}}{\rho \alpha^{2-n}}, \quad Nu = \frac{hL}{k} \quad (16)$$

The displacement is observed along the x and y axis whereas the displacement rate along the axis is denoted by u and v , respectively. The overall temperature of the domain

is denoted by T , $T = T_h$ represents the thermal heating, whereas the cold temperature is symbolized as $T = T_C$. The kinematic viscosity and the thermal diffusivity are indicated by ν and α . Moreover, pressure and density are indicated by p and ρ , respectively. In addition to this, the above horizontal surfaces (s_1 and s_2), the curves (c_1 , c_2 and c_3) and the vertical walls (l_1 and l_2) of the fin are also highlighted in Figure 1.

3. Numerical Computation

The current work deals with heat and its relation to energy and the physical attributes of a power-law fluid. The power-law fluid is also recognized as an Ostwald-de Waele relationship and is a generalized Newtonian fluid i.e., a time-independent non-Newtonian fluid useful for approximating the behavior of a non-Newtonian fluid. For instance, one case shows a drop in viscosity with an upsurge in shear rate, acknowledged as shear thinning behavior and categorizing the fluid as pseudoplastic fluid. Another example depicts the Newtonian conduct for constant fluid viscosity, whereas the less common dilatant fluid viscosity increases along with an increasing rate of shear stress, giving rise to shear thickening behavior. The process of natural convection is taking place in the domain due to the provided temperature variation through sinusoidal (non-uniform) heating of the inserted flipper. The consideration of the above-mentioned circumstances leads to the formation of coupled partial differential expressions represented in Equations (10)–(13). A very useful approach to discretize the governing equations is the Galerkin finite element method. Hybrid meshing comprises elements with three to four vertices. In this regard, the quadratic interpolation functions interpose the momentum and heat transportation in the flow domain whereas, to introduce the pressure constraints, linear interpolating polynomials are used. Meshing at coarser level is executed in Figure 2 to show variation in degrees of freedom and elements formations.

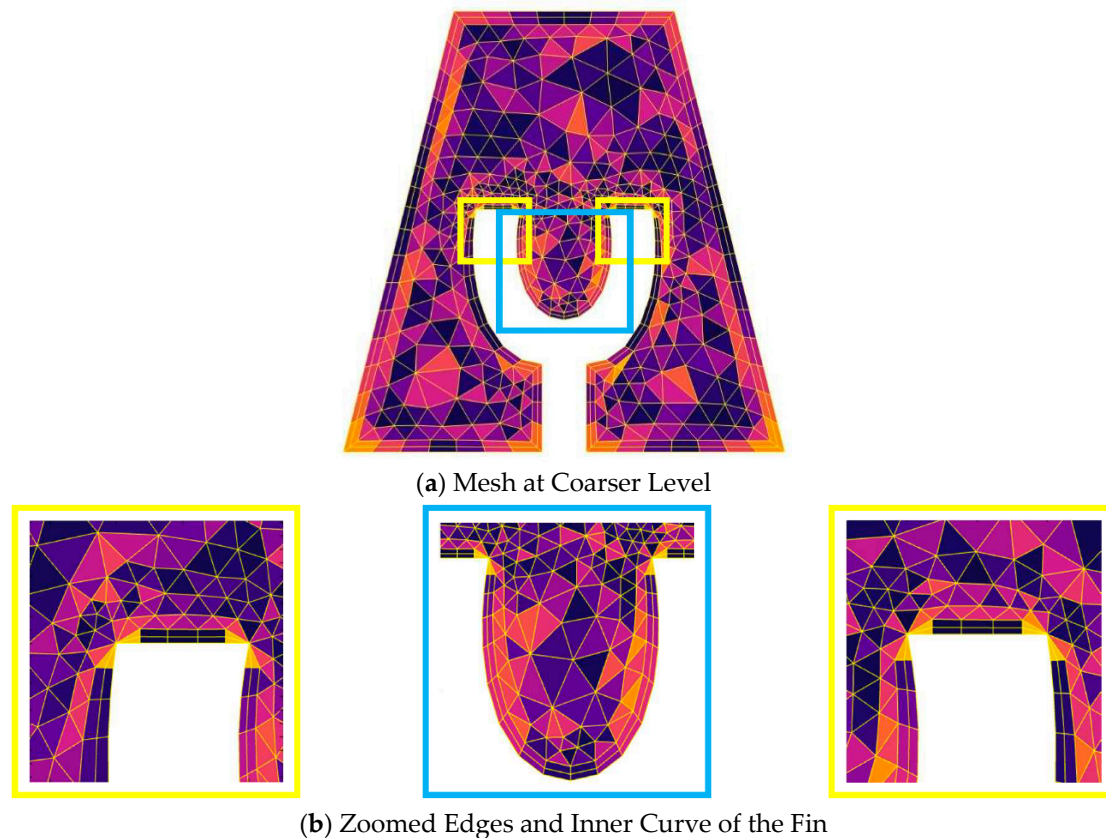


Figure 2. Represents the coarser refinement level showing the discretized flow domain and the inclusion of $P_2 - P_1$ elements of a triangular and quadrilateral nature.

4. Results and Discussion

According to the mathematical modeling for natural convective heat transfer in a power-law liquid enclosed in a trapezoidal in contact with a heated U-shaped fin, a study was piloted to apprehend the effect of governing parameters on the phenomenon.

Table 1 gives the number of elements and the degree of freedom for different levels of refinement. One of the key methods for achieving results is the discretization of the region through the method of finite element. In the above table, an ascending order of refinement levels (*R.L*) from extremely coarse to extremely fine is given, which shows that incrementing levels increases the total number of elements. The number of triangles and quads in the discretized domain is also listed. The power-law index (*n*) is a suitable mathematical expression to relate kinetic energy of fluid to the intensity of momentum generated in the fluid due to natural convection.

Table 1. Number of elements and degree of freedom for different refinement levels (*R.L*'s).

Refinement Level (<i>R.L</i>)	Number of Triangles	Number of Quads.	Number of Elements	Degree of Freedom
<i>R.L</i> (1)	296	112	408	1172
<i>R.L</i> (2)	479	158	637	1768
<i>R.L</i> (3)	736	208	944	2532
<i>R.L</i> (4)	1331	306	1637	4212
<i>R.L</i> (5)	1973	378	2351	5856
<i>R.L</i> (6)	3088	472	3560	8556
<i>R.L</i> (7)	8507	958	9465	21,824
<i>R.L</i> (8)	22,901	1822	24,723	54,932
<i>R.L</i> (9)	27,407	1822	29,229	63,944

Named after Wilhelm Nusselt, a German engineer, the Nusselt number signifies the transmission of heat within a fluid owing to convection. In the current study, the U-shape embedded inside the trapezoidal domain is heated non-uniformly, generating the heat flux. The change in the heat flux under the provision of sinusoidal heating is observed against the Rayleigh number (*Ra*) in Table 2. The range of the parameter chosen to measure the variations in local Nusselt number is $10^4 \leq Ra \leq 10^6$. It can be observed from the tabulation that by fixing $n = 1$ and $Pr = 5$, an uplift in the diffusivity of momentum is seen with the increment in the Rayleigh number, because with the increment in (*Ra*), the degree of buoyancy forces an increment and lifts the local convective heat transfer coefficient. The table also describes the change in (*K.E*) concerning variation in (*Ra*). It can be seen from the table that an abrupt increase in (*K.E*) occurs as we increase the value of (*Ra*) from 1E4 to 1E6. Since the increment in Rayleigh number (*Ra*) leads to a decrease in the viscosity of the fluid to decrease, as an outcome the energy of the fluid molecules increase rapidly. The value of (*K.E*) for $10^4 \leq Ra \leq 10^6$ is tabulated in the above table. A rapid intensification in the motion energy is seen at $Ra = 1 \times 10^6$, i.e., $K.E = 25737$.

Table 2. Variation in kinetic energy for different values of the power-law index (*n*).

Rayleigh Number (<i>Ra</i>)	Heat Flux (<i>Nu</i>)	Kinetic Energy (<i>K.E</i>)
10,000	5.8026	89.774
1.0000×10^5	7.4054	2637.4
1.0000×10^6	12.129	25,737

Table 3 provides information regarding energy generation by the virtue of the fluid's motion following the increase in the viscosity of the fluid. The variation in the (*n*) ranges from $0.5 \leq n \leq 1.5$ by fixing (*Ra*) = 1000 and (*Pr*) = 5. Under the influence of non-uniform heating of the flipper, it is evaluated that, with proliferation in (*n*) the kinetic energy decreases within the flow region. This is because of the fact that increasing (*n*)

causes the viscosity of the fluid to escalate, and hence results in reducing its velocity. As a result, the average kinetic energy of the fluid molecules depreciates.

Table 3. Variation in Nusselt number (Nu) and kinetic energy at different values of Rayleigh number (Ra).

Power-Law Index (n)	Kinetic Energy ($K.E$)
0.5	206.28
1	0.33140
1.5	0.038054

Analyzing the influence of (n) on the fluid circulation leads to significant observations described in Figure 3. The power-law catalog ' n ' characterizes the relation among the constituents of stress and strain rate tensors. The characterization is categorized into three cases. In the case <1 , the shear thinning agrees with the description of pseudo-plastic fluids, i.e., reduction in viscosity with an increment in strain rate. The second case $n = 1$ terms a fluid as a Newtonian fluid, whereas the case $n > 1$ designates the shear thickening, describing the dilatant conduct of a fluid, i.e., increasing viscosity with increasing strain rate. The influence of the motion of a power-law fluid upon convective heat transfer via natural convection, initiated by non-uniform heating of a U-shaped fin placed in a two dimensional trapezoidal cavity, is studied in the above figure. It is seen clearly that in Figure 3, as n increases and changes the fluid state from shear thinning to shear thickening, the liquid circulation decreases and the number of streamlines drops, reflecting the slowdown of the convective fluid flow. Figure 3a describes the pseudo plastic inheritance of the fluid which is defined as the decrease in viscidness with the intensification in strain rate. This case is also termed as shear thinning when $n < 1$. Certainly, it can be observed that the lesser the viscosity, the more the fluid flow is enhanced. Four vortices are formed, two at the sides below the fin (at c_1 and c_2) and two above it (at s_1 and s_2). At this point, the vortices are circular describing the intensified fluid velocity or circulation. The reason is that, in cases where the fluid displays shear thinning behavior, its viscosity is comparatively much less. Hence, the fluid exhibits rotatory motion in the cavity above and at the sides of the fin. Furthermore, Figure 3b,c represents the fluid flow against the magnitude of the power-law index, being equal to and greater than unity respectively. In both cases, the fluid motion consists of four vortices, but the circular shape of whirlpools is disrupted and they have attained parabolic structures. Figure 3c shows slightly more ruptured structures than Figure 3b. Since the increment in (n) defines the increase in the viscidness of the fluid, the fluid motion decreases and the circular patterns slow down to give parabolic outlines.

Figure 4 is illustrated to describe the distribution of momentum against $10^4 \leq Ra \leq 10^6$, fixing $n = 1$ and $Pr = 5$. From Figure 4a–c, (Ra) is incremented and displayed. It can be seen that the parabolic (near c_1 and c_2) and circular (above s_1 and s_2) patterns deform and show compactness on the inner boundary lining of the cavity and the fin. The increase in (Ra) gives way to the temperature distribution and the buoyancy forces in order to lift their magnitude. Hence, the increase in the stream profile of a power-law fluid shows the behavior illustrated in Figure 4.

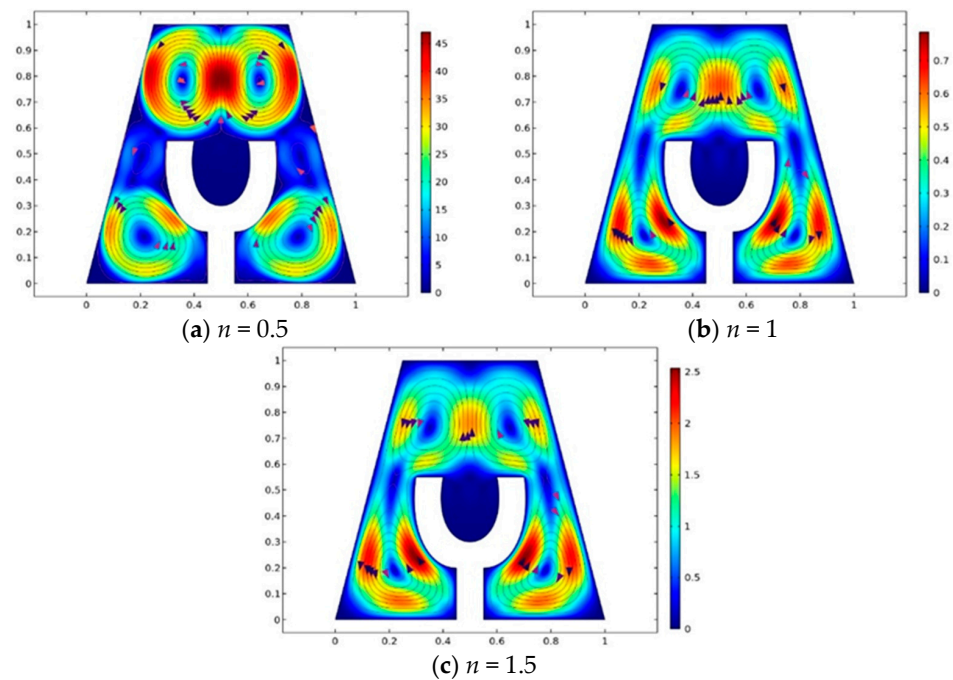


Figure 3. Velocity profiles and streamlines for varying power law index (n) for $Ra = 1000$ and $Pr = 5$.

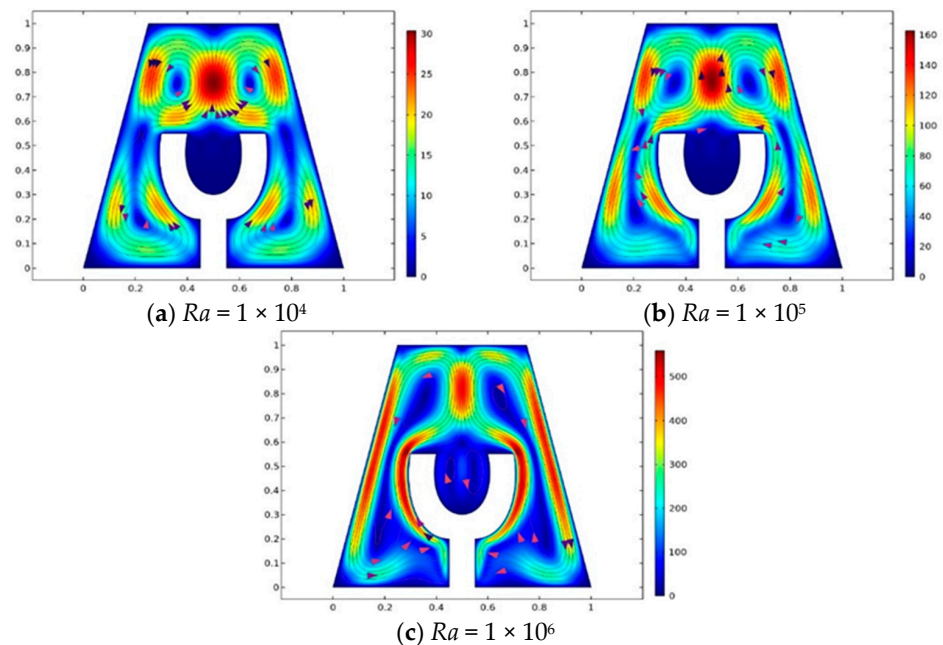


Figure 4. Velocity profiles and streamlines for varying Rayleigh number (Ra) at $n = 1$ and $Pr = 5$.

The above Figure 5 is portrayed to highlight the thermal distribution in the fluid against $10^4 \leq Ra \leq 10^6$, fixing $n = 1$ and $Pr = 5$. It can be explicitly interpreted from Figure 5 that by uplifting the magnitude of (Ra) under the influence of non-uniform heating from the fin surface, an increasing sharpness is visualized near its edges and curves. Since non-uniform or sinusoidal heating is provided, by uplifting (Ra) the isothermal curves initially showed heat transport in parabolic curves, and gradually all the heat compacted against the fin's walls and at its center (near c_3). Moreover, an increasing (Ra) gives rise to the inertial forces of the liquid molecules depending upon the temperature difference.

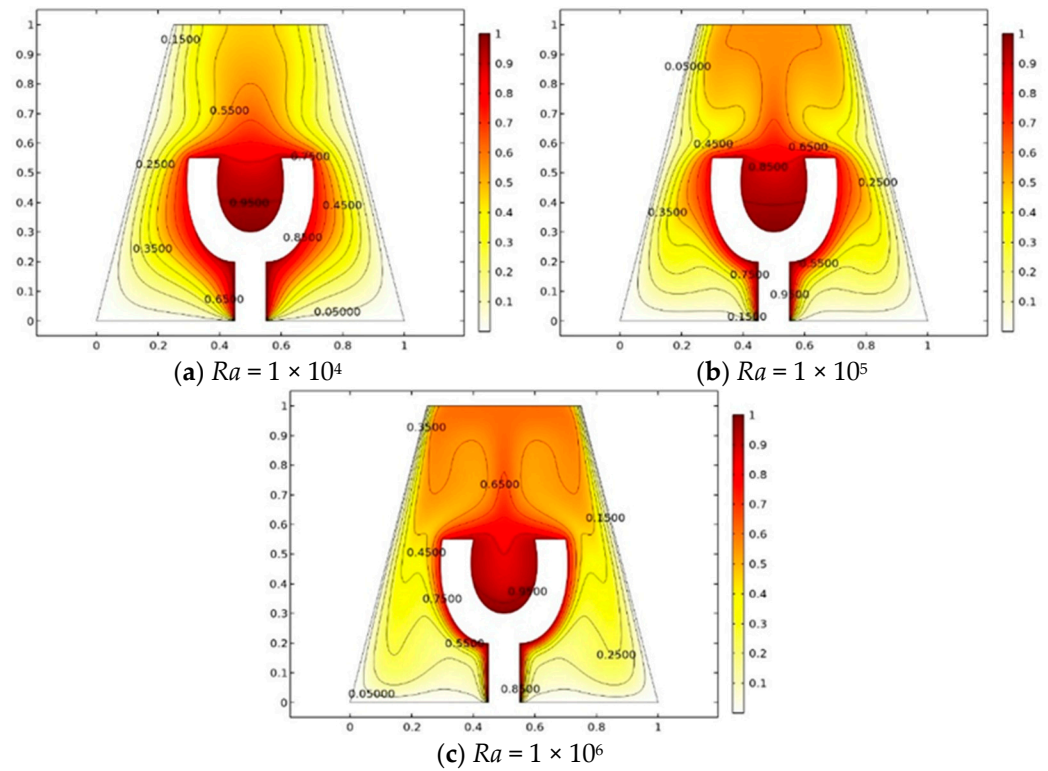


Figure 5. Temperature profile and isothermal contours for varying (Ra) at $n = 1$ and $Pr = 5$.

Sliding values of kinetic energy concerning the power-law index $0.5 \leq n \leq 1.5$ are encapsulated in Figure 6. Comparatively, the maximum value of kinetic energy is attained for $n < 1$, i.e., the velocity of the fluid is at a maximum due to lessened viscosity. Furthermore, the graph is abruptly decreased and attained a constant value of ($K.E$) for ($n \geq 1$), giving off a straight line analogous to the x -axis. Since the mobility of the fluid particle lowers, as an outcome the motion of the fluid molecules reduces and ($K.E$) drops down.

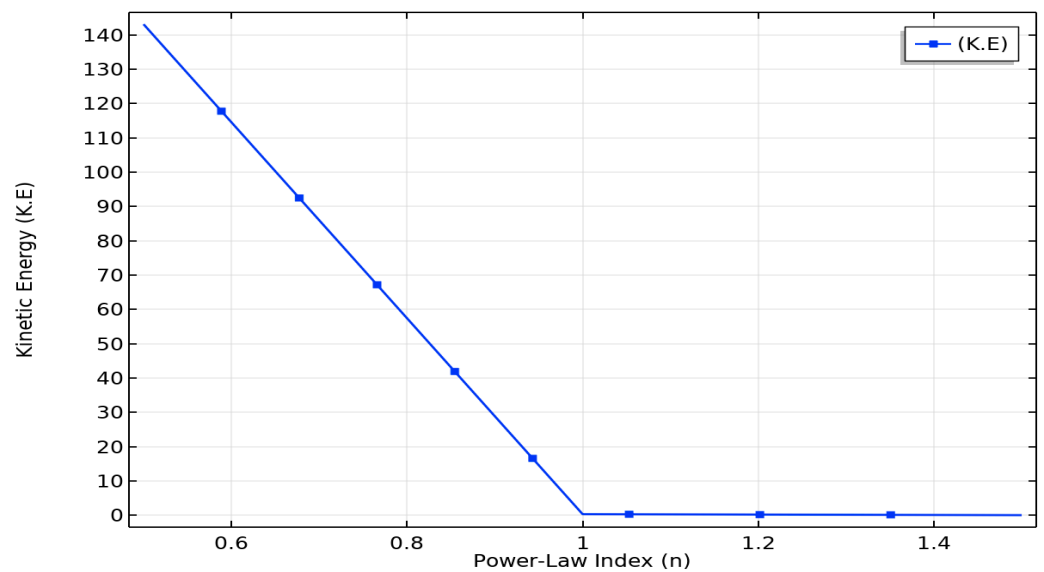


Figure 6. Graphical demonstration of variation in kinetic energy w.r.t power law index (n).

Figure 7 is the demonstration of the influence of (Ra) on the energy exhibited by the particles due to their motion. In the range $10^4 \leq Ra \leq 10^6$, as the Rayleigh number

is increased, the inertial forces of the molecules also increase, dominating the viscous forces, hence the kinetic energy increases. From the graph, a straight line is attained and proportional behavior is observed.

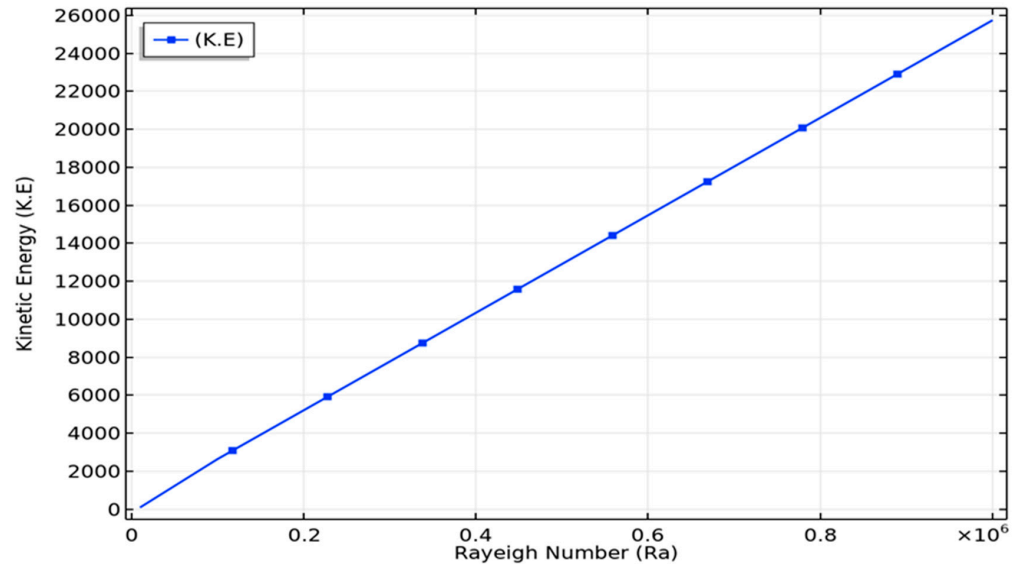


Figure 7. Graphical demonstration of variation in kinetic energy and w.r.t Rayleigh number (Ra).

The concept regarding the increase in the heat flux due to increment in (Ra) can be visualized in Figure 8. The proliferation in (Ra) results in heat manifestation and hence causes the buoyancy forces to take charge. Therefore, the Nusselt number increases in profile. Initially from 0 to 0.1, an abrupt rise in (Nu) occurs, while after a certain point the value increases proportionally.

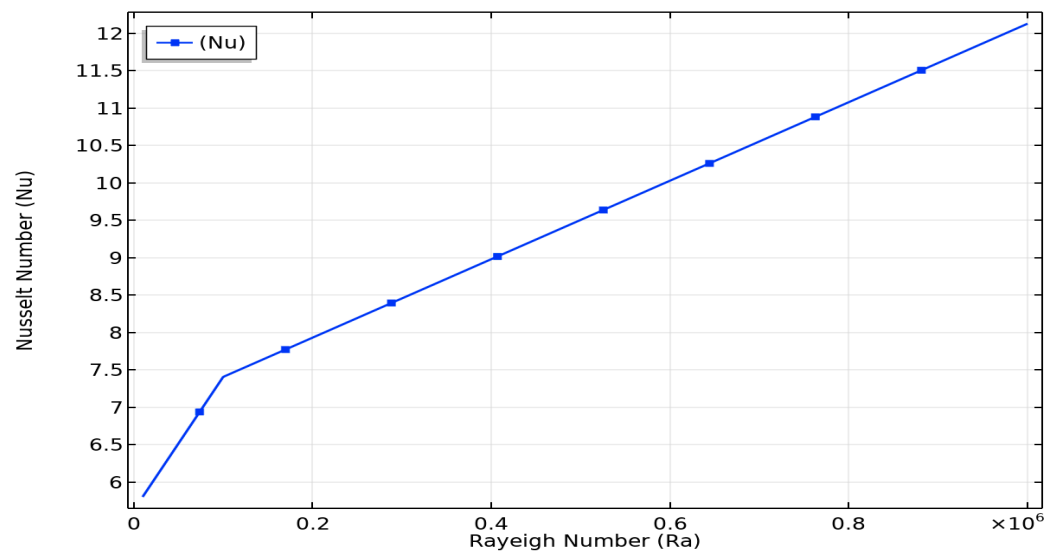


Figure 8. Graphical demonstration of variation in Nusselt number (Nu) and w.r.t Rayleigh number (Ra).

Variation in the vertical constituent of the velocity by drawing a cutline at $y = 0.5$ is analyzed in Figure 9a. From the overview of the sketch, it is seen that velocity along the cutline varies in the waveform. In addition, two wave structures are formed, one before the interaction of the fluid with a U-shaped fin, and the other after the passage of fluid to the obstruction. From the attained structures, it is seen that velocity behaves oppositely for

the concerned cases. It is worthwhile to mention that absolute maxima of curves is attained at $x = 0.17$ and $x = 0.63$, while absolute minima are attained at $x = 0.04$ and $x = 0.71$.

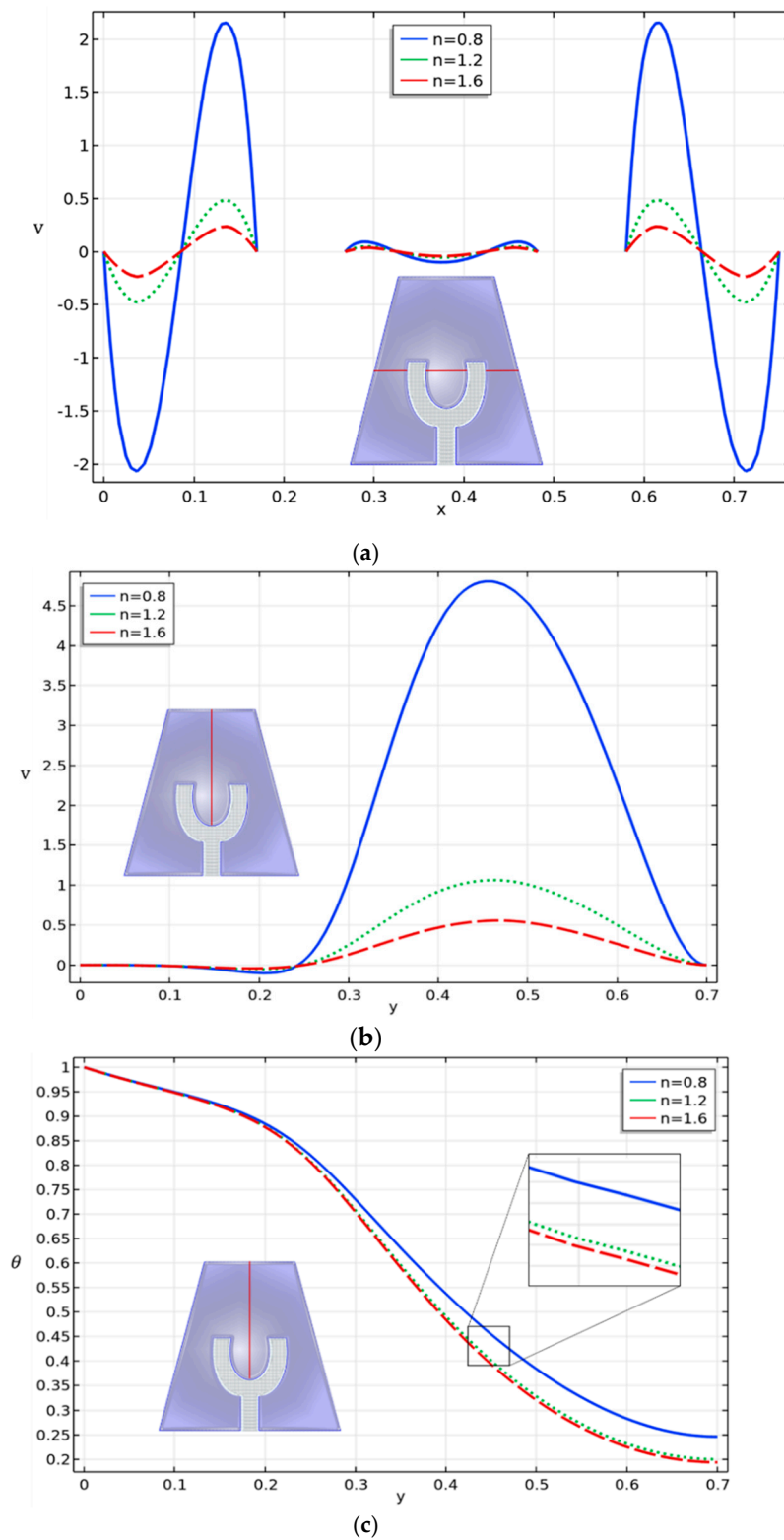


Figure 9. (a) Cutlines for v component of velocity for different values of power law index (n) at $y = 0.5$. (b) Cutlines for v component of velocity for different values of power law index (n) at $x = 0.5$. (c) Cutlines for temperature distribution θ for different values of power law index (n) at $x = 0.5$.

Figure 9b describes the variation in the horizontal component of the velocity w.r.t varying y . It is clear from the illustration that initially the velocity of the liquid at zero forms $y = 0$ to $y = 0.15$, whereas from $y = 0.3$ the graphical lines show an abrupt increase and show inverted parabolic curves.

Maximum intensification is attained for the shear-thinning case at $y = 0.45$. Furthermore, Figure 9c reveals the behavior of thermal distribution for varying x and fixed $y = 0.5$. From the figure, it is depicted that, at the center of the fin, the magnitude of heat is maximum whereas it declines as the value of y increases. Three curved graphs are represented for the shear thinning, Newtonian, and shear thickening cases. As viscosity is lesser in the pseudoplastic fluids, an observable gap is seen in the lines representing the thermal distribution, comprising of larger values for $n < 1$ at every instant than for that of $n \geq 1$.

5. Conclusions

This research is conducted to show the characteristics of motion of fluid in a trapezoidal cavity containing a non-uniformly U-shaped fin. Mathematical rheological modeling is constructed and presented as partial differential expressions. The Galerkin finite element technique is applied to deal with the computational complexity in the flow domain. Tabulation of several elements comprising quadrilaterals and triangles is presented to describe the discretization of the domain. Circular, parabolic and compact curves have been observed in the momentum distribution and heat transportation graphs. Furthermore, solutions regarding the problem are gained via the Finite Element Method for non-uniform thermal difference when varying Rayleigh number (Ra) and power-law index (n).

The central deductions are given below:

- a. Increasing magnitude of (Ra) results in increased magnitude of kinetic energy, i.e., energy associated with the motion of the fluid particles.
- b. The heat flux increases with the increase in Rayleigh number (Ra).
- c. The fluid flow circulations are greatly affected by the increase in (Ra) and (n). As the degree of (Ra) increases, velocity increases, whereas opposite behavior is seen for increasing values of (n).
- d. The kinetic energy for the shear-thinning case of the fluid decreases, whereas an abrupt increase is seen as the magnitude of the power-law index increments.
- e. Table graphs for the kinetic energy and Nusselt number are illustrated against the Rayleigh number and power-law index.

Author Contributions: Conceptualization, S.B.; data curation, M.R. and H.A.; formal analysis, A.A.; investigation, A.A.; methodology, A.A. and H.A.; software, S.B.; writing—original draft, S.N. and M.R.; Review S.N.; Funding, A.A.; writing—review and editing, H.A. and S.B. All authors have read and agreed to the published version of the manuscript.

Funding: This research received no external funding.

Institutional Review Board Statement: Institutional Review Board Statement and approval number is not applicable.

Informed Consent Statement: No informed consent statement is required for this study.

Data Availability Statement: All data is available in manuscript.

Conflicts of Interest: The authors declare no conflict of interest.

Nomenclature

u, v	Velocity components
ρ	Fluid density
p	Fluid pressure
g	Gravity

β	Thermal expansion coefficient
T	Fluid temperature
n	Power-law index
T_c	The temperature of the cold wall
Ra	Rayleigh number
Pr	Prandtl number
$K.E.$	Kinetic energy

References

1. Alebrahim, A.; Bejan, A. Constructal trees of circular fins for conductive and convective heat transfer. *Int. J. Heat Mass Transfer* **1999**, *42*, 3585–3597. [[CrossRef](#)]
2. Almogbel, M.; Bejan, A. Cylindrical trees of pin fins. *Int. J. Heat Mass Transfer* **2000**, *43*, 4285–4297. [[CrossRef](#)]
3. Kraus, A.D.; Aziz, A.; Welty, J.R. *Extended Surface Heat Transfer*; John-Wiley: New York, NY, USA, 2002.
4. Lorenzini, G.; Biserni, C.; Isoldi, L.A.; Santos, E.D.D.; Rocha, L.A.O. Constructal design applied to the geometric optimization of Y-shaped cavities embedded in a conducting medium. *J. Electron. Packag.* **2011**, *133*, 041008. [[CrossRef](#)]
5. Lorenzini, G.; Rocha, L.A.O. Geometric optimization of TY-shaped cavity according to constructal design. *Int. J. Heat Mass Transfer* **2009**, *52*, 4683–4688. [[CrossRef](#)]
6. Abdi, A.; Martin, V.; Chiu, J.N. Numerical investigation of melting in a cavity with vertically oriented fins. *Appl. Energy* **2019**, *235*, 1027–1040. [[CrossRef](#)]
7. Bendaraa, A.; Charafi, M.M.; Hasnaoui, A. Numerical study of natural convection in a differentially heated square cavity filled with nanofluid in the presence of fins attached to walls in different locations. *Phys. Fluids* **2019**, *31*, 052003. [[CrossRef](#)]
8. Goodarzi, H.; Akbari, O.A.; Sarafraz, M.M.; Karchegani, M.M.; Safaei, M.R.; Shabani, G.A.S. Numerical simulation of natural convection heat transfer of nanofluid with Cu, MWCNT, and Al₂O₃ nanoparticles in a cavity with different aspect ratios. *J. Therm. Sci. Eng. Appl.* **2019**, *11*, 061020. [[CrossRef](#)]
9. Shi, X.; Khodadadi, J.M. Laminar natural convection heat transfer in a differentially heated square cavity due to a thin fin on the hot wall. *J. Heat Transfer* **2003**, *125*, 624–634. [[CrossRef](#)]
10. Horbach, C.d.S.; Santos, E.D.d.; Isoldi, L.A.; Rocha, L.A.O. Constructal design of Y-shaped conductive pathways for cooling a heat-generating body. *Defect Diffus. Forum* **2014**, *348*, 245–260. [[CrossRef](#)]
11. Rehman, K.; Kouz, W.A.; Sherif, E.S.; AbdelMalek, Z. Hybrid meshed analysis on rhombus shaped solid material domain (RSSMD) equipped with non-Newtonian liquid stream. *J. Sci. Adv. Mater. Devices* **2020**, *5*, 476–486. [[CrossRef](#)]
12. Tavana, M.; Pourmehran, O.; Aghaei, A.; Sangara, J.A. Mofid Gorji-Bandpy, Numerical Analysis of Fluid Flow and Heat Transfer in Microchannels with Various Internal Fins. *Int. J. Artif. Intell. Mechatron.* **2015**, *3*, 2320–5121.
13. Scozia, R.; Frederick, R.L. Natural Convection in Slender Cavities with Multiple Fins Attached on an Active Wall. *Numer. Heat Transfer* **1991**, *20*, 127–158. [[CrossRef](#)]
14. Facas, G.N. Natural Convection in a Cavity with Fins Attached to Both Vertical Walls. *J. Thermophys. Heat Transfer* **1993**, *7*, 555–560. [[CrossRef](#)]
15. Nag, A.; Sarkar, A.; Sastri, V.M.K. Natural Convection in a Differentially Heated Square Cavity with a Horizontal Partition Plate on the Hot Wall. *Comput. Methods Appl. Mech. Eng.* **1993**, *110*, 143–156. [[CrossRef](#)]
16. Ozoe, H.; Churchill, S.W. Hydrodynamic stability and natural convection in Ostwald–de Waele and Ellis fluids: The development of a numerical solution. *AIChE J.* **1972**, *18*, 1196–1207. [[CrossRef](#)]
17. Kaddiri, M.; Naïmi, M.; Raji, A.; Hasnaoui, M. Rayleigh Benard convection of non-Newtonian power-law fluids with temperature-dependent viscosity. *ISRN Thermodyn.* **2012**, *2012*, 614712. [[CrossRef](#)]
18. Kim, G.B.; Hyun, J.M.; Kwak, H.S. Transient buoyant convection of a power-law non-Newtonian fluid in an enclosure. *Int. J. Heat Mass Transf.* **2003**, *46*, 3605–3617. [[CrossRef](#)]
19. Lamsaadi, M.; Naïmi, M.; Hasnaoui, M. Natural convection heat transfer in shallow horizontal rectangular enclosures uniformly heated from the side and filled with non-Newtonian power law fluids. *Energy Convers. Manag.* **2006**, *47*, 2535–2551. [[CrossRef](#)]
20. Lamsaadi, M.; Naïmi, M.; Hasnaoui, M.; Mamou, M. Natural convection in a tilted rectangular slot containing non-Newtonian power-law fluids and subject to a longitudinal thermal gradient. *Numer. Heat Transf. Part A Appl. Int. J. Comput. Methodol.* **2006**, *50*, 561–583. [[CrossRef](#)]
21. Turan, O.; Sachdeva, A.; Chakraborty, N.; Poole, R.J. Laminar natural convection of power-law fluids in a square enclosure with differentially heated side walls subjected to constant temperatures. *J. Non-Newton. Fluid Mech.* **2011**, *166*, 1049–1063. [[CrossRef](#)]
22. Ternik, P.; Rudolf, R. Laminar natural convection of non-Newtonian nanofluid in a square enclosure with differentially heated side walls. *Int. J. Simul. Modeling* **2013**, *12*, 5–16. [[CrossRef](#)]
23. Turan, O.; Sachdeva, A.; Poole, R.J.; Chakraborty, N. Aspect ratio and boundary conditions effects on laminar natural convection of power-law fluids in a rectangular enclosure with differentially heated side walls. *Int. J. Heat Mass Transf.* **2013**, *60*, 722–738. [[CrossRef](#)]
24. Ternik, P.; Buchmeister, J. Buoyancy-induced flow and heat transfer of power law fluids in a side heated square cavity. *Int. J. Simul. Modeling* **2015**, *14*, 238–249. [[CrossRef](#)]

25. Alloui, Z.; Vasseur, P. Natural convection of Carreau–Yasuda non-Newtonian fluids in a vertical cavity heated from the sides. *Int. J. Heat Mass Transf.* **2015**, *84*, 912–924. [[CrossRef](#)]
26. Ouertatani, N.; Cheikh, N.B.; Beya, B.B.; Lili, T. Numerical simulation of two-dimensional Rayleigh–Bénard convection in an enclosure. *Comptes Rendus Mécanique* **2008**, *336*, 464–470. [[CrossRef](#)]
27. Kumari, M.; Pop, I.; Takhar, H.S. Free-convection boundary-layer flow of a non-Newtonian fluid along a vertical wavy surface. *Int. J. Heat Fluid Flow* **1997**, *18*, 625–631. [[CrossRef](#)]
28. Lewandowski, W.M.; Radziemska, E.; Buzuk, M.; Bieszk, H. Free convection heat transfer and fluid flow above horizontal rectangular plates. *Appl. Energy* **2000**, *66*, 177–197. [[CrossRef](#)]
29. Jordán, J.Z. Numerical study of an unsteady free convective magnetohydrodynamic flow of a dissipative fluid along a vertical plate subject to a constant heat flux. *Int. J. Eng. Sci.* **2006**, *44*, 1380–1393. [[CrossRef](#)]
30. Jha, B.K.; Ajibade, A.O. Free convective flow of heat generating/absorbing fluid between vertical porous plates with periodic heat input. *Int. Commun. Heat Mass Tran.* **2009**, *36*, 624–631. [[CrossRef](#)]
31. Jha, B.K.; Samaila, A.K.; Ajibade, A.O. Transient free-convective flow of reactive viscous fluid in vertical tube. *Math. Comput. Model.* **2011**, *54*, 2880–2888. [[CrossRef](#)]
32. Ahmed, J.; Mahmood, T.; Iqbal, Z.; Shahzad, A.; Ali, R. Axisymmetric flow and heat transfer over an unsteady stretching sheet in power law fluid. *J. Mol. Liq.* **2016**, *221*, 386–393. [[CrossRef](#)]
33. Al-Kouz, W.; Alshare, A.; Alkhalidi, A.; Kiwan, S. Two dimensional analysis of low pressure flows in the annulus region between two concentric cylinders. *Springer Plus* **2016**, *5*, 529. [[CrossRef](#)]
34. Shahzad, A.; Ali, R.; Hussain, M.; Kamran, M. Unsteady axisymmetric flow and heat transfer over time-dependent radially stretching sheet. *Alexandria Eng. J.* **2017**, *56*, 35–41. [[CrossRef](#)]
35. Ahmed, J.; Shahzad, A.; Begum, A.; Ali, R.; Siddiqui, N. Effects of inclined Lorentz forces on boundary layer flow of Sisko fluid over a radially stretching sheet with radiative heat transfer. *J. Braz. Soc. Mech. Sci. Eng.* **2017**, *39*, 3039–3050. [[CrossRef](#)]
36. Mishra, S.R.; Khan, I.; Al-Mdallal, Q.M.; Asifa, T. Free convective micropolar fluid flow and heat transfer over a shrinking sheet with heat source. *Case Stud. Therm. Eng.* **2018**, *11*, 113–119. [[CrossRef](#)]
37. Khan, M.; Salahuddin, T.; Malik, M.Y.; Khan, F.; Hussain, A. Variable diffusion and conductivity change in 3d rotating Williamson fluid flow along with magnetic field and activation energy. *Int. J. Numer. Methods Heat Fluid Flow* **2019**, *30*, 2467–2484. [[CrossRef](#)]
38. Sakinder, S.; Salahuddin, T.; Fahad, S.; Al-Mubaddel, S.; Alam, M.M.; Ahmad, I. Influence of entropy generation on hybrid nanoparticles near the lower region of solid sphere. *Case Stud. Therm. Eng.* **2021**, *26*, 101–123. [[CrossRef](#)]
39. Lin, P.; Ghaffari, A. Steady flow and heat transfer of the power-law fluid between two stretchable rotating disks with non-uniform heat source/sink. *J. Therm. Anal. Calorim.* **2020**. [[CrossRef](#)]
40. Lin, P.; Gaffari, A. Mustafa, A theoretical analysis of steady three-dimensional flow and heat transfer of Power-Law nanofluid over a stretchable rotating disk filled with gyrotactic microorganisms. *Phys. Scr.* **2020**, *96*, 015008.
41. Ghaffari, A.; Kausar, S. Numerical solution of the partial differential equations that model the steady three-dimensional flow and heat transfer of Carreau fluid between two stretchable rotatory disks. *Numer. Methods Partial. Differ. Equ.* **2020**. [[CrossRef](#)]
42. Khan, M.I.; Shah, F.; Khan, S.U.; Ghaffari, A.; Chu, Y.M. Heat and mass transfer analysis for bioconvective flow of Eyring Powell nanofluid over a Riga surface with nonlinear thermal features. *Numer. Methods Partial. Differ. Equ.* **2020**. [[CrossRef](#)]
43. Usman, W.; Khan, I.; Badruddin, A.; Gaffari, A.; Ali, H.M. Heat transfer in steady slip flow of tangent hyperbolic fluid over the lubricated surface of a stretchable rotatory disk. *Case Stud. Therm. Eng.* **2021**, *24*, 100825. [[CrossRef](#)]
44. Ahmad, H.; Alam, N.; Omri, M. New computational results for a prototype of an excitable system. *Results Phys.* **2021**, *11*, 104666. [[CrossRef](#)]
45. Goodarzi, M.; Safaei, M.R.; Karimipour, A.; Hooman, K.; Dahari, M.; Kazi, S.N.; Sadeghinezhad, E. Comparison of the Finite Volume and Lattice Boltzmann Methods for Solving Natural Convection Heat Transfer Problems inside Cavities and Enclosures. In *Abstract and Applied Analysis*; Hindawi: London, UK, 2014. [[CrossRef](#)]
46. Pordanjani, A.H.; Aghakhani, S.; Karimipour, A.; Afrand, M.; Goodarzi, M. Investigation of free convection heat transfer and entropy generation of nanofluid flow inside a cavity affected by magnetic field and thermal radiation. *J. Therm. Anal. Calorim.* **2019**, *137*, 997–1019. [[CrossRef](#)]
47. Yousefzadeh, S.; Rajabi, H.; Ghajari, N.; Sarafraz, M.M.; Akbari, O.M.; Goodarzi, M. Numerical investigation of mixed convection heat transfer behavior of nanofluid in a cavity with different heat transfer areas. *J. Therm. Anal. Calorim.* **2020**, *140*, 2779–2803. [[CrossRef](#)]
48. Goodarzi, M.; D’Orazio, A.; Keshavarzi, A.; Mousavi, S.; Karimipour, A. Develop the nano scale method of lattice Boltzmann to predict the fluid flow and heat transfer of air in the inclined lid driven cavity with a large heat source inside, Two case studies: Pure natural convection & mixed convection. *Phys. A Stat. Mech. Appl.* **2018**, *509*, 210–233. [[CrossRef](#)]
49. Aghaei, A.; Sheikhzadeh, G.A.; Goodarzi, M.; Hasani, H.; Damirchi, H.; Afrand, M. Effect of horizontal and vertical elliptic baffles inside an enclosure on the mixed convection of a MWCNTs-water nanofluid and its entropy generation. *Eur. Phys. J. Plus* **2018**, *133*, 486. [[CrossRef](#)]
50. Goodarzi, M.; Safaei, M.R.; Oztop, H.F.; Karimipour, A.; Sadeghinezhad, E.; Dahari, M.; Kazi, S.N.; Jomhari, N. Numerical Study of Entropy Generation due to Coupled Laminar and Turbulent Mixed Convection and Thermal Radiation in an Enclosure Filled with a Semitransparent Medium. *Sci. World J.* **2014**. [[CrossRef](#)]

-
51. Rasool, G.; Khan, W.A.; Bilal, S.M.; Khan, I. MHD squeezed Darcy–Forchheimer nanofluid flow between two h–distance apart horizontal plates. *Open Phys.* **2020**, *18*, 1100–1107. [[CrossRef](#)]
 52. Rozati, S.A.; Montazerifar, F.; Akbari, O.A.; Hoseinzadeh, S.; Nikkhah, V.; Marzban, A.; Abdolvand, H.; Goodarzi, M. Natural convection heat transfer of water/Ag nanofluid inside an elliptical enclosure with different attack angles. *Math. Methods Appl. Sci.* **2020**. [[CrossRef](#)]
 53. Raisi, A. Natural Convection of Non-Newtonian Fluids in a Square Cavity with a Localized Heat Source. *Stroj. Vestn. J. Mech. Eng.* **2016**, *62*, 10. [[CrossRef](#)]